THE JOURNAL OF PHYSICAL CHEMISTRY C

Article

Cite This: J. Phys. Chem. C 2018, 122, 5578−5589

pubs.acs.org/JPCC

Reversal of Paramagnetic Effects by Electron Spin Saturation

Sheetal K. Jain,[†,∥] Ting A. Siaw,[†,∥,⊥] Asif Equbal,[†] Christopher B. Wilson,[‡] Ilia Kaminker,[†] and Songi Han*[,†,§]

[†]Department of Chemistry and Biochemistry, [‡]Department of Physics, and [§]Department of Chemical Engineering, University of California Santa Barbara, Santa Barbara, California 93106-9510, United States

Supporting Information

ABSTRACT: We present a study in which both significant dynamic nuclear polarization (DNP) enhancement of ^{7}Li NMR and reversal of the paramagnetic effects (PEs) are achieved by microwave (μw) irradiation-induced electron spin saturation of nitroxide radicals at liquid-helium temperatures. The reversal of the PE was manifested in significant narrowing of the ^{7}Li NMR line and reversal of the paramagnetic chemical shift under DNP conditions. The extent of the PE was found to decrease with increased saturation of the electron paramagnetic resonance line, modulated as a function of microwave (μw) power, frequency, duration of irradiation, and gating time between μw irradiation and NMR detection. The defining observation was the shortening of the electron phase memory time, T_m, of the excited observer spins with increasing μw irradiation and concurrent electron spin saturation of the electron spin bath. This and a series of corroborating studies reveal the origin of the NMR line narrowing to be the reversal of paramagnetic relaxation enhancement (PRE), leading us to debut the term REversal of PRE by electron Spin SaturatION (REPRESSION). The shortening of electron T_m of any paramagnetic system as a function of electron spin saturation has not been reported to date, making REPRESSION a discovery of this study. The reversal of the paramagnetic dipolar shift is due to the decrease in electron spin order, also facilitated by electron spin saturation. This study offers new fundamental insights into PE under DNP conditions and a method to detect and identify NMR signal proximal to paramagnetic sites with reduced or minimal line broadening.

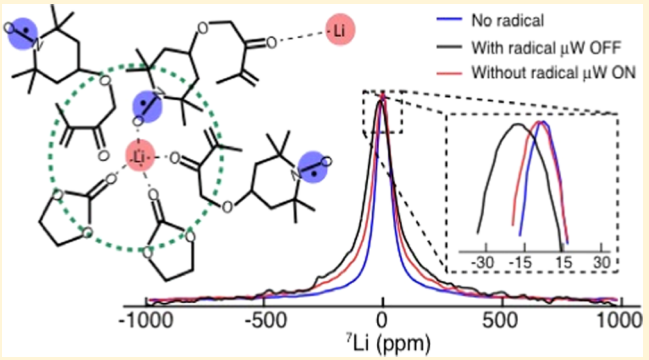

INTRODUCTION

Dynamic nuclear polarization (DNP) is gaining a foothold in the field of materials characterization as a sensitivity enhancement technique for nuclear magnetic resonance (NMR) experiments.[1−12] In particular, for surface characterization of materials, DNP is proving to be potentially transformative[1,13,14] by overcoming the low sensitivity of NMR and reducing the bulk signal contribution from the core material. In DNP, often an exogenous source of unpaired electrons that we refer to as "DNP agents" is embedded into the material of interest, typically by dissolving stable nitroxide radicals or other paramagnetic molecules in the solvent. The transfer of polarization from the highly polarized electron spins of the DNP agent to the nuclear spins is achieved by microwave (μw) irradiation under the right conditions and typically at cryogenic temperatures, resulting in NMR signal enhancements by up to several orders of magnitude.

In the last two decades, DNP has witnessed a rapid progress in the synthesis of radical-based DNP agents,[15−24] optimization of solvent condition,[25−27] μw instrumentation,[28−35] and theoretical understanding[36−49] to improve the performance of DNP. Despite the advancements made in the field of DNP, the underlying mechanisms for the electron to nuclear spin polarization transfer under various experimental conditions and the effect of the paramagnetic spins and μw irradiation on the NMR spectra are not fully understood. Significant challenges remain in the field of DNP, but the one that we address here is the detection of accurate NMR signal proximal to the paramagnetic DNP agents, exogenous or endogenous. The presence of paramagnetic DNP agents may significantly broaden and/or shift the NMR signal, which is particularly problematic for the pursuit of achieving localized NMR characterization in the vicinity of site-specifically anchored, surface-adsorbed, or otherwise localized paramagnetic DNP agents. Besides, the spin physics underlying the paramagnetic effects (PEs) on the NMR line shape and shift under cryogenic and DNP conditions is not well understood.

The line broadening, signal quenching, and peak shifting of the NMR signal result from the hyperfine interactions, dipolar or scalar, between the electron (e) and nuclear (n) spins present in the sample of interest, together referred to as paramagnetic effects (PEs) here. The NMR line broadening can result from two different mechanisms. First, from a coherent evolution of the spin system in the presence of large hyperfine

Received: January 10, 2018
Revised: February 20, 2018
Published: February 21, 2018

DOI: 10.1021/acs.jpcc.8b00312
J. Phys. Chem. C 2018, 122, 5578−5589

couplings, and second, from the paramagnetic relaxation enhancement (PRE) caused by incoherent fluctuations in the local magnetic fields of the electron spins at the nuclear spin sites. The former mechanism depends on the strength of the coupling interaction, i.e., the gyromagnetic ratio, the distance between the electron and nuclear spins, and their relative orientation. The second mechanism depends on not only the coupling strength but also the correlation time of the local field fluctuations caused by the electron spins at the nuclear spin site. Therefore, the two mechanisms are fundamentally different from each other. The peak shifting in the NMR signals, known as paramagnetic dipolar shifts in NMR or pNMR shifts or shielding,[50−52] is caused by either contact shift (CS) or pseudocontact shift (PCS). The CS originates from the isotropic Fermi contact (FC) interaction, whereas the PCS is caused by anisotropic dipolar interactions.[53] The PRE and PCS effects are routinely exploited to aid in NMR-based structural studies of biomolecules.[54] However, the relatively high concentrations (10−20 mM) of the paramagnetic probes used as DNP agents and cryogenic temperatures under typical DNP conditions may lead to additional quenching of the NMR peaks in their vicinity, with compromised resolution and ambiguity in peak assignments.[55]

Because of the aforementioned reasons, the decoupling of the e−n interaction is an important objective in DNP.[55,56] We note that in standard solid-state NMR under magic angle spinning (MAS), high-power proton decoupling is routinely employed to enhance the NMR resolution of heteronuclei.[57−61] Hyperfine decoupling has also been used in electron paramagnetic resonance (EPR) for enhancing resolution and correlation spectroscopy techniques.[62−64] However, these experiments are not routinely employed under DNP conditions to improve NMR resolution through e−n decoupling. The challenge of achieving e−n decoupling begins with the challenge of effectively manipulating the electron spins over the whole width of the EPR line with the available μw power. At high magnetic fields (>3 T), the EPR line of a typical nitroxide radical-based DNP agent spans up to 1 GHz due to the anisotropy of the electron g-factor and hyperfine coupling of the nitroxide's electron spin to the ^{14}N nuclear spin (I = 1). The presence of both the secular and pseudosecular hyperfine coupling terms in the e−n coupling Hamiltonian, variation in electron spin relaxation rates across the EPR spectrum, and the presence of electron spectral diffusion make e−n decoupling a complex process to understand and control. The μw power limitation can be overcome to an extent by using a microwave resonator that can achieve a higher effective B_1 field with lower powers. This, in combination with shaped pulses generated by arbitrary waveform generator (AWG), can achieve broad-band EPR saturation[65] that should lead to e−n decoupling. However, such an approach has yet to be tested. Recently, Barnes and coworkers have demonstrated line narrowing by up to ∼48 Hz from 419 to 371 Hz of ^{13}C NMR spectra of urea in the presence of 40 mM trityl OX063 radical in DNP juice at 90 K and under MAS. In this work, frequency-swept μw irradiation with a sweep width of ±43 MHz, centered around the maximum of the trityl EPR spectrum at 197.64 GHz, was used during NMR acquisition with 5 W output power (ω_1 = 0.38 MHz) to demonstrate electron decoupling.[66] An alternative method to achieve significant electron saturation with low μw power is to utilize favorable electron spin relaxation parameters and/or to exploit strongly coupled electron spin manifolds. Feasibilities of such scenarios have in fact been forecasted in the literature. Hovav et al.[67] and Siaw et al.[35] showed that in the presence of high radical concentrations (>5 mM) at low temperatures (4−20 K) a significant portion of the EPR line can be saturated using μw powers of $O(10^1-10^2)$ mW at magnetic fields exceeding 3 T, as recently demonstrated by mapping out the EPR profile under DNP conditions by pump-probe electron double resonance (ELDOR) at 7 T.[68] These studies have ascribed the observed saturation to long electron spin−lattice relaxation times (T_{1e}) and efficient spectral diffusion that maximize the integral electron spin saturation.[68] The current study closely exploits this mechanism.

In this study, we demonstrate for the first time the observation of the REversal of Paramagnetic Relaxation Enhancement by electron Spin SaturatION (REPRESSION). The experiments are carried out under DNP conditions in a frozen glass sample of a common Li-ion battery electrolyte solution of 1.0 M $LiPF_6$ dissolved in a 1:1 ethylene carbonate/dimethyl carbonate (EC/DMC) solvent mixture doped with two different nitroxide radicals. A systematic examination of the impact of radical concentration, μw irradiation parameters, and temperature on the REPRESSION effect is presented. Additionally, an analysis of the extent of EPR saturation by ELDOR and the modulation of electron spin relaxation times with varying μw parameters have been performed to understand the effect of electron spin saturation on the REPRESSION effect. Critically, we demonstrate that T_m is modulated by the saturation of the EPR spectrum that depresses the electron spin polarization of the spin bath from close to 100% at 4 K or 45% at 20 K to smaller values, offering the key empirical basis for the REPRESSION effect. We also observe effects of μw irradiation on the chemical shifts of ^{7}Li NMR spectra, following similar time constants and dependencies as seen with REPRESSION. Without going into a detailed analysis, we briefly discuss that in the regime where the high-temperature approximation is no longer valid, the total magnetic susceptibility is significantly affected by the saturation of the electron spins,[53] leading to the reversal of the pNMR shifts. For clarity, we refer to the combination of REPRESSION and revival of the original chemical shift values as the REversal of Paramagnetic Effects ALtogether (REPEAL) in the conclusion of this study.

EXPERIMENTAL SECTION

Hardware for NMR, EPR, and DNP Measurements. The DNP−NMR experiments under varying concentrations of the radicals shown in Figures 1 and S1 were all performed using a 7 T WB NMR magnet. Because of changes in hardware, the magnet was charged to 6.9 T for the DNP, ELDOR, T_{1e}, and T_m measurements, as presented in Figures 2−7. Because this field change had to occur at an advanced stage of these studies, we report measurements at two different fields, but all critical measurements that support our conclusions were performed at 6.9 T. All experiments were conducted using a Bruker Avance DSX spectrometer and a home-built microwave bridge operating in a quasi-optical (QO) setup, partially designed by Thomas Keating Ltd.[35] The bridge was powered with a solid-state source (Virginia Diodes, Inc.) with 120 mW output and tunable across 190−198 GHz for the 6.9 T experiments (140 mW and 193−201 GHz for the 7 T experiments). A home-built DNP probe equipped with a corrugated waveguide for the microwave transmission and saddle coil tuned at 114.27 MHz with an inductively coupled rectangular loop was used for detecting the ^{7}Li NMR signal. Cryogenic temperatures (∼4 K)

DOI: 10.1021/acs.jpcc.8b00312
J. Phys. Chem. C 2018, 122, 5578−5589

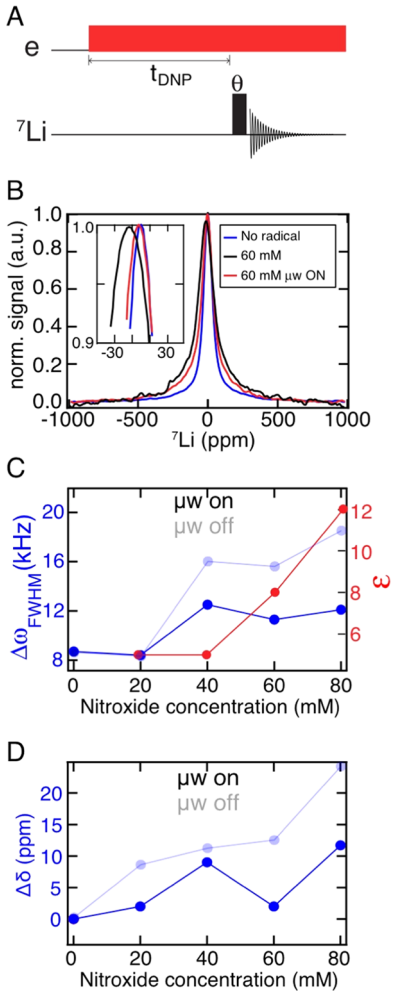

Figure 1. (A) Pulse sequence used to record DNP-enhanced ^{7}Li NMR spectra. (B) ^{7}Li NMR spectra recorded without addition of any radical (blue), with 60 mM 2,2,6,6-tetramethylpiperidinyloxyl methacrylate (TEMPOmet) (black) and 60 mM TEMPOmet under μw irradiation (red). The inset shows the zoomed in version of the spectra to highlight the line width and chemical shift differences. (C) $\Delta\omega_{FWHM}$ (blue) and ε (red) are plotted as a function of radical concentration for both μw on and off cases. (D) $\Delta\delta$ as a function of radical concentration for μw on and off cases. See the parameters in Experimental Section.

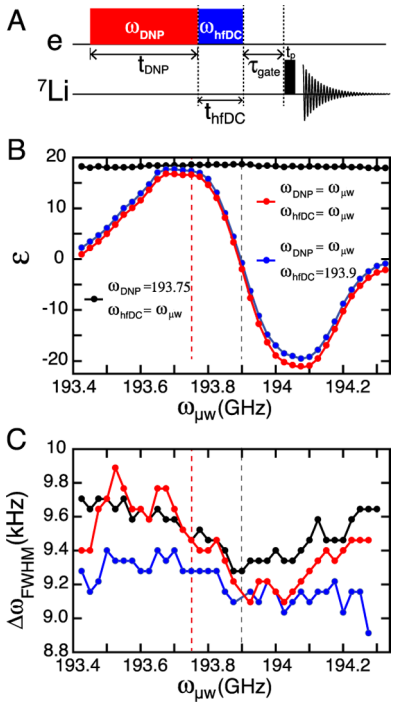

Figure 2. (A) Pulse sequence used for DNP−NMR experiments. A detailed description of all of the blocks is given in the text. (B) Signal enhancements at 4 K temperature and 6.9 T magnetic field as a function of μw frequency are plotted with t_{DNP} + t_{hfDC} = 60 s, μw power ($P_{\mu w}$) = 120 mW, gating time (τ_{gate}) = 0 s. Red and blue data points are collected while varying the μw frequency during DNP (ω_{DNP}) while hyperfine decoupling (hfDC) frequency (ω_{hfDC}) set to ω_{DNP} and 193.9 GHz, respectively. The black data points represent the case with μw frequency varied during the hfDC block while fixing the DNP buildup block frequency to 193.75 GHz. The red data points are shifted vertically downward for the sake of visibility. (C) ^{7}Li NMR line widths for the experiments shown in (B) with same color coding. The vertical dashed lines indicate the positions of maximum enhancement (red) and maximum hfDC (black). All of the experiments were performed on the Li-electrolyte sample doped with 60 mM TEMPOmet radical.

were achieved using a custom STVP-200-NMR continuous-flow liquid-helium cryostat (Janis Research Co., LLC). A Sogevac SV65VB rotary vane pump (Oerlikon Leybold Vacuum) was used to create vacuum in the sample chamber to further reduce the temperature below the liquid-helium boiling point. The desired temperature was maintained with the help of a voltage-controlled resistive heater and a Cernox temperature sensor (Lake Shore Cryotronics), which were controlled by a LabView program using a proportional integral derivative algorithm. To perform ELDOR experiments, the pulse-forming unit of the 194 GHz QO DNP/EPR system operational at 6.9 T was selected between two separate solid-state microwave synthesizers, which allowed for the generation of pulses at two different microwave frequencies within the same pulse sequence.[35,65]

Experimental Parameters. The pulse sequence for the experiments presented in Figures 2−5 is shown in Figure 2A. The default μw parameters were set as follows, unless mentioned otherwise in the figure caption: μw frequency ($\omega_{\mu w}$), 193.7 MHz; power ($P_{\mu w}$), 120 mW; irradiation time (t_{DNP}), 60 s; and gating (τ_{gate}), 0 s. The temperature was 4 K for all experiments except the ones shown in Figure 3, in which we

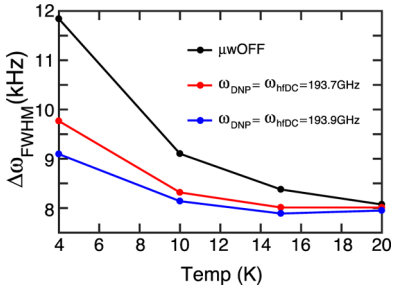

Figure 3. ^{7}Li NMR line widths, $\Delta\omega_{FWHM}$, are plotted at different temperatures without any μw irradiation (blue), with 60 s μw irradiation at frequency 193.7 GHz that yield maximum DNP enhancement (black) and at frequency 193.9 GHz that yield optimum hfDC effects (red). The sample used was Li-electrolyte solution doped with 60 mM TEMPMOmet radical. The remaining parameters are given in Experimental Section.

DOI: 10.1021/acs.jpcc.8b00312
J. Phys. Chem. C 2018, 122, 5578−5589

vary the temperature. A radio frequency (RF) pulse of 2 μs with 20 dB power attenuation to a 300 W initial power was used for NMR detection of the ^{7}Li spins. The μw irradiation was turned off during detection of the NMR signal in all experiments except the ones shown in Figure 1, in which the reversal of the PE were first observed with continuous wave (CW) (Figure 1A). In the ELDOR experiments (see Figure 6A for the pulse sequence), changes in the two-pulse echo intensity at the ω_{probe} frequency were monitored as a function of the ω_{pump} frequency. The experimental parameters were: t_p = 750 ns; τ = 600 ns; τ_d = 10 μs, and t_{pump} = 100 or 500 ms with the corresponding repetition times of 500 or 900 ms. The ω_{pump} frequency was stepped between 193.1 and 194.6 GHz in 153 steps, ω_{probe} was set to 193.7 GHz, 10 shots per step were collected for signal averaging, and a two-step phase cycle (0, 180°) was employed such that the total experimental times were 25.5 and 45.9 min for the two ELDOR experiments. T_{1e} and T_m measurements shown in Figures 6C and 7 were performed using the same pulse sequence as for ELDOR (Figure 6A). In the case of T_{1e} measurement using saturation recovery sequence, the pump pulse length (t_{pump}) was set to 100 ms, ω_{pump} = ω_{probe}, and the remaining parameters were unchanged from the ELDOR experiments except τ_d, which was varied from 10 μs to 2800.01 ms in steps of 200 ms. For the T_m measurements, we denote t_{pump} as t_{DNP}, τ_d as τ_{gate}, and the μw power during the pump pulse as $P_{\mu w}$ to be consistent with the naming convention used for the DNP−NMR experiments. The default values for t_{DNP}, τ_{gate}, and $P_{\mu w}$ were 500 ms, 50 ms, and 120 mW, respectively, for the T_m experiments shown in Figure 7. For each T_m data set, 32 points were collected, during which the time delay between the echo pulses (τ) was varied between 50 ns and 2 μs on a logarithmic scale. The decay curves were fit to a stretched exponential of the form $\exp(-(2\tau/\tau_M)^x)$ with x = 3/2 using MATLAB, following Edwards et al.[69] The reported values for T_m are the average decay times given by $T_m = \Gamma(1 + 1/x)\tau_M$.[70]

Sample Preparation. The Li^+-ion electrolyte solution comprising 1.0 M lithium hexafluorophosphate ($LiPF_6$) in 50/50 v/v solution of ethylene carbonate (EC) and dimethyl carbonate (DMC) was purchased from Sigma-Aldrich. The stable nitroxide radicals, either 2,2,6,6-tetramethylpiperidinyloxyl (TEMPO) or TEMPO methacrylate (TEMPOmet) purchased from Sigma-Aldrich, were added in the required amount by weight to obtain the desired radical concentration. After dissolving the radical in the Li-ion electrolyte solution, 50 μL of it was pipetted into a cylindrical Delrin or Kel-F (chlorotrifluoroethylene) sample cup with inner and outer diameters of 5.3 and 7 mm, respectively, and height of 8 mm. The sample solution was not degassed or otherwise treated to remove oxygen. After packing the sample cup with the Li-ion solution, the sample cup was covered using a Kel-F cap and sealed with vacuum grease (Apiezon N-grease) or Teflon tape on the edges of the cap to minimize exposure of the electrolyte solution to air. Each sample was prepared on the day of the experiment and cooled to cryogenic temperatures within 15−30 min of sample preparation to avoid interactions of the electrolyte solution with air moisture.

RESULTS

We begin by describing the observation of ^{7}Li NMR spectra of 1.0 M $LiPF_6$ dissolved in a 1:1 ethylene carbonate/dimethyl carbonate (EC/DMC) solvent mixture doped with TEMPOmet at concentrations ranging between 0 and 80 mM. The data were acquired at 7 T and 4 K. The equivalent experiments were also repeated with TEMPO instead of TEMPOmet as the DNP agent, and the results are shown in the Supporting information (SI) (Figure S1). The experimental setup is described in Experimental Section.

The pulse sequence for the DNP−NMR experiments is shown in Figure 1A, which consists of CW μw irradiation with 140 mW power at a frequency of 197.8 GHz (optimum for DNP) for a 60 s buildup duration, followed by NMR detection with a short tilt pulse of angle θ (μw irradiation is turned off during NMR detection). The NMR spectra comparing the ^{7}Li NMR signals from the Li-electrolyte solution without any radical (blue), in the presence of 60 mM TEMPOmet without μw irradiation (black) and in the presence of 60 mM TEMPOmet with μw irradiation (red), are shown in Figure 1B. A significant line broadening (i.e., change in the NMR line width at half-maximum, $\Delta\omega_{FWHM}$), as well as peak shifting ($\Delta\delta$ = δ(no radical) − δ(radical)) in the presence of the radical is observed, as highlighted in the inset of Figure 1B. The spectrum shown as the red curve demonstrates the reversal of the PE, encompassing both line broadening and peak shifting, as a result of μw irradiation. From the results acquired at various radical concentrations shown in Figure 1, it becomes evident that at higher concentrations (above 20 mM), the PE can make drastic changes in the line widths and peak positions. For example, in the presence of 80 mM TEMPOmet, $\Delta\omega_{FWHM}$ is broadened from 9 to 18 kHz and the peak shifted by 25 ppm (see the faded blue data points in Figure 1C,D).

The signal enhancement (ε) at various radical concentrations is shown in Figure 1C as red data points plotted along the right y axis, together with the NMR line width at half-maximum ($\Delta\omega_{FWHM}$) as blue data points along the left y axis, with μw irradiation on (solid) and off (faded). The parameter ε is the ratio of μw on to μw off NMR signal with recycle delay of 60 s. The peak shifting, $\Delta\delta$, is shown in Figure 1D as blue data points with μw irradiation on (solid) and off (faded). Under μw irradiation with maximal CW power available in our setup, we observe ^{7}Li NMR line narrowing from 18 down to 11 kHz and a significant reversal of the paramagnetic chemical shift by ∼14 ppm out of the total 25 ppm shift observed. Thus, the PE that originates from the hyperfine coupling interactions is truncated/reversed by μw irradiation, indicating an occurrence of hyperfine decoupling (hfDC). The following experiments are designed to systematically dissect the origin and mechanism of this dramatic observation of apparent hfDC effects, achieved with relatively low μw powers. In all of the remaining experiments, we used the Li-electrolyte solution doped with 60 mM TEMPOmet as the sample, which shows significant reversal of the chemical shift (∼11 ppm) and line narrowing of ∼3 kHz from 12.5 to 9.5 kHz under μw irradiation. The absolute values are slightly altered from those in Figure 1 moving forward due to an irreversible replacement of the superconducting magnet with change in the field strength from 7 to 6.9 T, change in the probe circuit, and the use of a new batch of sample, midway through the studies (repeating these would incur prohibitively high research costs). However, these changes do not affect the discussions of the results or conclusions.

The next set of experiments is designed to confirm whether the reversal of the PE is actually caused by the original hfDC mechanism or is a manifestation of the reweighting of the NMR signals due to higher DNP enhancements for remote nuclear spins relative to the paramagnetic sites, here the DNP agents.

DOI: 10.1021/acs.jpcc.8b00312
J. Phys. Chem. C 2018, 122, 5578−5589

With these experiments, we also check the influence of temperature and see if heating generated by μw irradiation can lead to our apparent observations. We tackle these questions by essentially figuring out whether the observed NMR line narrowing and peak shifting follow the trends of DNP signal enhancements or not and whether we can achieve different NMR line narrowing effects by switching the μw irradiation frequency during the hfDC time, t_{hfDC}, before NMR detection (see Figure 2A). If temperature was the main modulator of the observed effect, shifting the μw irradiation frequency during t_{hfDC} should not affect the resulting PE.

Figure 2A shows the pulse sequence used to record DNP-enhanced ^{7}Li NMR spectra as a function of the μw parameters. The pulse sequence can be divided into four blocks: (i) bulk nuclear polarization buildup block, during which μw irradiation is applied for time t_{DNP} at frequency ω_{DNP} (shown in red), (ii) hfDC block, in which the frequency of the μw irradiation (show in blue) is switched to ω_{hfDC} to maximize the reversal of the PE, (iii) gating block is a delay without any μw or RF irradiation applied that allows for the recovery of the PE and decay of the NMR signal following T_{1n}, and (iv) NMR detection block consisting of a short RF pulse to tilt the nuclear polarization for NMR acquisition.

Figure 2B,C shows ε and $\Delta\omega_{FWHM}$ as a function of μw irradiation frequency ($\omega_{\mu w}$), respectively, upon the application of the polarization buildup block (ω_{DNP}) and the hfDC block (ω_{hfDC}), but no gating block. The red data points show ε (Figure 2B) and $\Delta\omega_{FWHM}$ (Figure 2C) plotted against $\omega_{\mu w}$, where Figure 2B represents a regular DNP frequency profile, in which $\omega_{\mu w}$ was varied concurrently with ω_{DNP} and ω_{hfDC} (i.e., $\omega_{\mu w} = \omega_{DNP} = \omega_{hfDC}$). In other words, these data points in red correspond to the result of standard DNP experiments without any frequency switch effects during the experiment. This affects the ^{7}Li NMR signal enhancement in an expected manner. However, the trend in the ^{7}Li NMR $\Delta\omega_{FWHM}$ is noteworthy as the NMR lines are narrowest around the μw frequency of $\omega_{\mu w} \sim 193.9$ GHz (in Figure 2C) that is at the weighted center of the EPR spectrum compared to other irradiation frequencies, and not at $\omega_{\mu w} \sim 193.75$ GHz that corresponds to one of the DNP enhancement maxima. Generally, the observed trend in $\Delta\omega_{FWHM}$ of the ^{7}Li NMR line (red data in Figure 2C) shows no correlation with the ^{7}Li NMR signal enhancements of a standard DNP profile, which already rules out the possibility of selective signal enhancements being responsible for the observed NMR line narrowing. To further confirm this, we next put an hfDC block at the end of the DNP buildup block with fixed $\omega_{hfDC} = 193.9$ GHz and varied $\omega_{\mu w} = \omega_{DNP}$ for the buildup block (blue data in Figure 2B). The DNP frequency profile remain unchanged because the hfDC block duration of $t_{hfDC} = 0.5$ s is negligible compared to the DNP buildup time t_{DNP} of 60 s but the NMR lines are narrower across all μw frequencies compared to those without the hfDC block at $\omega_{hfDC} = 193.9$ GHz (compare blue data to red data in Figure 2C). This shows that the hfDC block of the DNP pulse sequence is mostly responsible for the NMR line narrowing, not the much longer DNP buildup block. Finally, we vary ω_{hfDC} while keeping ω_{DNP} fixed at 193.75 GHz, which is the value that provides maximum positive DNP enhancement (black data, Figure 2). As expected, the DNP signal enhancement remains unaffected, while the $\Delta\omega_{FWHM}$ of the ^{7}Li NMR line (black data in Figure 2C) is still significantly altered. These data prove that the NMR line narrowing is uncorrelated with the DNP signal enhancements and thus it is not due to reweighting of the NMR signal toward remote nuclei from the paramagnetic sites. These observations also prove that the NMR line narrowing is not due to effects of μw-induced heating, as the three data sets shown in Figure 2 should display very similar sample heating effects from μw-induced irradiation, yet the NMR line narrowing shows distinct patterns consistent with the active decoupling of the paramagnetic effect from the proximal nuclei. The advantage of frequency switching during the hfDC block is highlighted by the vertical red dashed line in Figure 2B,C, which indicates that at the optimum DNP frequency $\omega_{DNP} = 193.75$ GHz the blue data point with $\omega_{hfDC} = 193.9$ GHz provides a line width narrowed by an additional ~350 Hz compared to the red data point collected without the frequency switch, i.e., $\omega_{hfDC} = \omega_{DNP} = 193.75$ GHz. We note that even at the edge of the frequency profile, the lines under μw irradiation are narrower compared to the μw off case; however, the line width recovers close to that without μw irradiation at $\omega_{\mu w}$ far out of the EPR line (see Figure S2 in SI), a peculiar phenomenon that requires future deliberations, but it is out of the scope of this study.

Next, we show that the hfDC effect is present at temperatures up to 20 K in the presence of 60 mM monoradical concentrations (see Figure 3). It is evident that the effect is more prominent at lower temperatures and diminishes at high temperatures. The black data points in Figure 3 correspond to the line widths without any μw irradiation, the red data points are measured with μw irradiation at $\omega_{\mu w} = 193.75$ GHz with $P_{\mu w} = 120$ mW for $t_{DNP} + t_{hfDC} = 60$ s, and the blue data points show the line widths using the same parameters, except the $t\omega_{\mu w}$ is set to 193.9 GHz. The line widths obtained at 4 K with μw irradiation are still narrower than the line widths at 10 K without μw irradiation. This implies that μw irradiation of 120 mW would have to increase the sample temperature by more than 6 K to get the observed line narrowing purely due to temperature effects, which is not plausible (see earlier discussion on the temperature stability). The origin of this temperature effect is rooted in the mechanism of T_m of highly concentrated or clustered radicals with a strong e−e network, where e−e flip-flop processes of the spin bath dominate T_m of the observer spin, an effect strongly modulated by temperature, as discussed later in more detail.

As it is confirmed that the observed effect is a result of the reversal of the PE caused by μw irradiation, we investigate the underlying mechanism by examining the effect of μw power ($P_{\mu w}$), μw buildup time (t_{DNP}), and μw gating time (τ_{gate}) on the buildup and decay of the hfDC effect, as manifested in the narrowing of $\Delta\omega_{FWHM}$ (shown in Figure 4). The changes in the NMR peak shift, $\Delta\delta$, as a function of the same μw parameters are shown in the SI (Figure S3).

Figure 4A shows that $\Delta\omega_{FWHM}$ monotonically decreases with increasing $P_{\mu w}$. At the maximum available μw power (120 mW) and $\omega_{\mu w} = 193.7$ GHz, line narrowing of about 2.5 kHz is observed compare to no μw irradiation. The signal enhancement shows the expected increase with power, as well as the signature of oversaturation at higher powers (>80 mW), as described in earlier studies of Han and co-workers.[68,71] The $\Delta\omega_{FWHM}$ decreases and ε increases with t_{DNP}, but at significantly different rates (Figure 4B); we note that in the calculation of ε the μw off signal intensity with a recycle delay of 60 s was used for all of the data points. Interestingly, a rapid narrowing of $\Delta\omega_{FWHM}$ by about ~2 kHz occurs within the first 500 ms of the t_{DNP} irradiation time, followed by a smaller and gradual line narrowing with longer t_{DNP} of up to 2 s (see Figure 4B, blue). The enhancement ε, on the other hand, increases

DOI: 10.1021/acs.jpcc.8b00312
J. Phys. Chem. C 2018, 122, 5578−5589

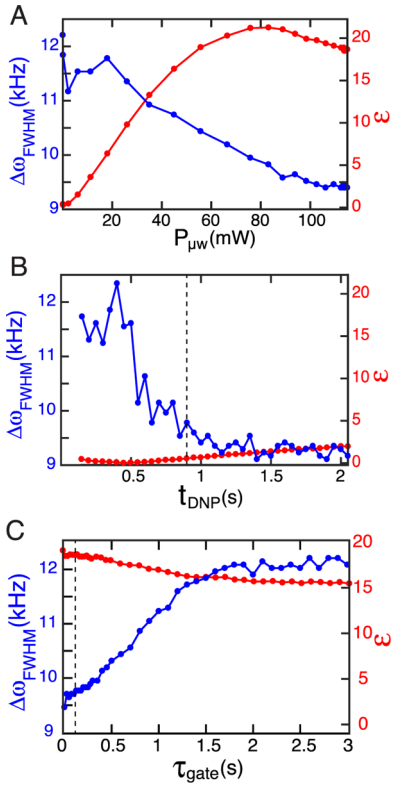

Figure 4. ^{7}Li NMR signal enhancements (red) and line widths (blue) recorded at 6.9 T magnet at 4 K temperature under static conditions as a function of μw parameters: (A) μw power, (B) irradiation time, and (C) gating period using the pulse sequence shown in Figure 2A on a sample of Li-electrolyte doped with 60 mM TEMPOmet. In all of the experiments, the μw frequency is fixed at 193.75 GHz and hfDC block time is set to 0 s. The vertical dashed lines indicate the similar $\Delta\omega_{FWHM}$ values at very different ε values obtained in gating and buildup experiments.

with a lower time constant with t_{DNP}, which is of the order of 10 s (red data points in Figure 4B). In other words, the hfDC effect builds up at a higher rate compared to the DNP enhancement. We note that the initial data points (t_{DNP} < 0.8 s) in Figure 4B correspond to tiny signals, making the accurate determination of the ^{7}Li NMR line widths difficult, and so leading to scattering of the absolute $\Delta\omega_{FWHM}$ values in the plot. Nonetheless, the trend is unambiguous.

Next, the gating period was varied. The results shown in Figure 4C demonstrate that when μw irradiation is turned off, the hfDC effect reverts and the line width increases back to the value when μw irradiation is off. The recovery to the fully broadened NMR line takes τ_{gate} of up to ~3 s, whereas the time constant for the recovery to the broadened ^{7}Li NMR line with μw gating is 0.98 s with 95% confidence bounds in range (0.82, 1.13). In other words, this reversal of the hfDC effect follows a longer time constant than the buildup of the hfDC effect featured in Figure 4B, which has a decay time constant for $\Delta\omega_{FWHM}$ of 0.23 s with a 95% confidence interval (0.16, 0.29 s). The simulated fitting curves with 95% confidence values for the line width as a function of t_{DNP} as well as τ_{gate} are shown in SI. Strikingly, the time constant for the recovery to the broadened ^{7}Li NMR line is longer than the electron T_{1e} (shown later), and significantly shorter than the nuclear spin−lattice relaxation time, T_{1n}, under these conditions of order $O(10^{3})$ s. These gating time-dependent data corroborate our earlier conclusion that the amount of NMR signal enhancement and the $\Delta\omega_{FWHM}$ line narrowing are not correlated. For example, $\Delta\omega_{FWHM}$ ~9.7 kHz is observed for $\varepsilon \sim 18$ when the gating delay is as short as τ_{gate} = 100 ms (Figure 4C), while the same $\Delta\omega_{FWHM}$ is measured for $\varepsilon \sim 1$ at a buildup time of $t_{DNP} \sim 0.9$ s (Figure 4B). The key observation is that the hfDC effect is not instantaneously turned off when the μw field of the hfDC block is turned off, as is the case with established decoupling schemes used in solid-state NMR.[58,59,61,72] This indicates that the reversal of the PE observed here is not a result of coherent averaging of the e−n interactions due to μw irradiation, as such effect would turn off instantaneously when μw irradiation is off. Coherent averaging also will require much greater μw power, as the e−n interactions can be as strong as of order $O(10^{1})$ MHz under the given experimental conditions, while our μw B_1 field is of order $O(10^{-1})$ MHz.

We note that line narrowing at short DNP buildup time (0.5 s) has been reported in the work by Barnes and co-workers,[66] where they see more dramatic effects of μw frequency switching on the NMR line width at shorter DNP buildup times. These observations were ascribed to the change in the average e−n distances during the buildup time, as the nuclear spin diffusion facilitates the flow of the polarization to the farther nuclear spins from the paramagnetic center. In our case, we also see a relatively rapid narrowing in $\Delta\omega_{FWHM}$ at short DNP buildup times with a time constant of 0.23 s, but additionally we see a slow recovery of $\Delta\omega_{FWHM}$ broadening after μw irradiation is turned off with a gating time constant of 0.98 s. To further investigate the role of the nuclear spin diffusion in this process, we plotted ^{7}Li NMR $\Delta\omega_{FWHM}$ against the μw gating time for different DNP buildup times (Figure 5). Remember that the

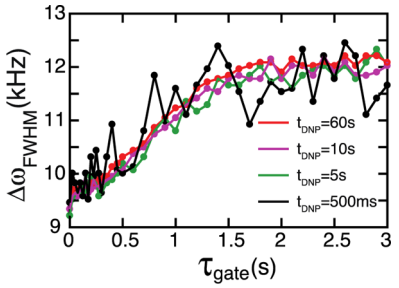

Figure 5. ^{7}Li NMR line widths of Li-electrolyte solution doped with 60 mM TEMPOmet as a function of gating period with different DNP buildup times: 60 s (red), 10 s (magenta), 5 s (green), and 0.5 s (black). The pulse sequence shown in Figure 1A was used with the default parameters given in the Experimental Section.

nuclear spin diffusion process is prevalent during the DNP buildup time; therefore, by controlling the buildup time, we can control the extent of nuclear spin diffusion. The results in Figure 5 reveal that the rate of attenuation of the apparent hfDC effect is independent of the DNP buildup time and hence independent of the propagation of nuclear spin diffusion.

So far, we have observed that $\Delta\omega_{FWHM}$ decreases with $P_{\mu w}$ and t_{DNP} and increases with τ_{gate}. These results suggest that EPR spin saturation caused by μw irradiation plays a key role in the hfDC mechanism, as the saturation varies in the same fashion with these μw parameters. Also, the observation of the "oversaturation" effect[71] demonstrated in the power dependence of the DNP enhancement that decreases above a threshold μw power value (Figure 4B) shows that the extent of EPR saturation under the experimental condition studied here is

DOI: 10.1021/acs.jpcc.8b00312
J. Phys. Chem. C 2018, 122, 5578−5589

significant. To directly verify that significant spectral diffusion is at play that drives the saturation of the EPR signal, two-frequency pump-probe ELDOR experiments were carried out using two different t_{pump} values, 100 and 500 ms. The pulse sequence for ELDOR is shown in Figure 6A, and the

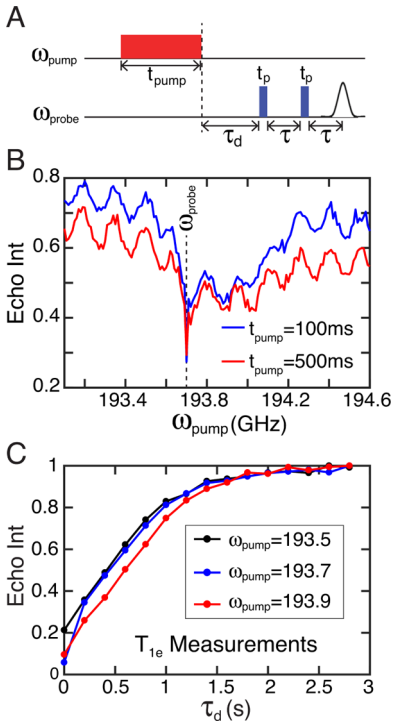

Figure 6. (A) ELDOR pulse sequence as described in Experimental Section. (B) ELDOR data, i.e., echo intensities as a function of the pump frequency while keeping the probe frequency fixed at 193.7 GHz (DNP maximum). Pump pulse lengths of 100 ms (blue) and 500 ms (red) were used with full μw power (120 mW) and delay τ_d = 10 μs. (C) Saturation recovery experiments recorded using the same pulse sequence by varying τ_d and keeping the remaining parameters same. The plots are shown for three pump frequencies, 193.5 GHz in black, 193.7 GHz in blue, and 193.9 GHz in red, with t_{pump} = 100 ms. The sample was Li-electrolyte solution doped with 60 mM TEMPOmet radical.

parameters are given in Experimental Section. The ELDOR data unequivocally show that a significant portion of the EPR line gets saturated, dampening the EPR signal over more than 400 MHz (spanning up to 800 MHz), even with μw irradiation of duration as short as t_{pump} = 100 ms (blue line, Figure 6B). Even greater saturation effects are observed with t_{pump} = 500 ms (red line, Figure 6B). We note that the periodic oscillations in the echo intensities are resulting from fluctuations in the effective μw powers at the sample position caused by standing waves at some particular frequencies in the current QO setup. Nonetheless, the ELDOR data unambiguously show that electron spectral diffusion is extremely efficient under the given experimental conditions, which can be ascribed to two factors: (i) long T_{1e} that gives sufficient time for the spectral diffusion to propagate and (ii) a strong e−e coupling network leading to faster spectral diffusion rates mediated by e−e flip-flop processes. In fact, we have experimental data that support the existence of both factors. T_{1e} values at several μw frequencies were measured by varying the gating time delay, τ_d, in the pulse sequence shown in Figure 6A. The data in Figure 6C show echo intensities as a function of τ_d delay at three different pump frequencies (ω_{pump} = 193.5, 193.7, and 193.9 GHz in black, blue, and red, respectively). The pump pulse length (t_{pump}) was set to 100 ms, and probe frequency to 193.7 GHz, while τ_d was varied from 10 μs to 2.8 s in steps of 200 ms. These parameters resulted in the acquisition of saturation recovery curves and yielded long T_{1e} of 0.67±0.15 s values. In addition, there is also a fast component of T_{1e}, which is detected by collecting data at small τ_d values, as shown in Figure S4, SI. This can be ascribed to effects of electron spectral diffusion, and hence is assigned a spectral diffusion time constant, T_{sd}.[71]

The observations so far suggest that significant saturation of the EPR spectrum plays a role in the apparent hfDC effect. However, the saturation recovery time according to T_{1e} of 0.67 s and the time constant for the recovery of the $\Delta\omega_{FWHM}$ with a gating time constant of 0.98 s do not exactly match. To analyze the mechanism behind the observed hfDC, we turn to the incoherent mechanism of paramagnetic line broadening. This hypothesis led us focus on factors that may modulate the time correlation of the e−n couplings.

It has been shown earlier that the T_m of the electron spins at very low temperature and high magnetic fields, governed by the e−e dipolar coupling-driven flip-flop dynamics.[69] This led us to measure T_m at various μw parameters to examine the correlation of the T_m and the apparent hfDC effect. The T_m data were recorded using the pulse sequence shown in Figure 6A (see Experimental Section). To mimic the DNP−NMR experimental conditions, the frequency of the pump pulse (i.e., ω_{pump}) was set to 193.75 GHz for maximal DNP and the detection frequency (ω_{probe}) was set to 193.9 GHz, as the goal was to see the effect of EPR saturation on the echo that is detected at a frequency, resulting in a maximal hfDC effect (Figure 2C). To our surprise, the T_m value indeed changes as a function of μw power, $P_{\mu w}$, as shown in Figure 7A (in black). Specifically, T_m decreased from 11 μs without μw irradiation to less than one-third of its value to 3 μs with μw irradiation with $P_{\mu w}$ = 120 mW. Such measurements, and consequently such observations, have never been reported to date. Figure 7A− C furthermore shows the trends of T_m (black data points) with μw power, irradiation time during DNP buildup, t_{DNP}, and gating time, τ_{gate}, respectively. This change in T_m is overlaid with the change in the ^{7}Li NMR line width, $\Delta\omega_{FWHM}$, acquired as a function of the same microwave parameters, as shown in Figure 7A−C, with blue data points (they are the same blue data points shown in Figure 4). A remarkable agreement in the trends for the changes in T_m and hfDC effects are observed, allowing us conclude that the hfDC effect is mediated by the shortening of the T_m relaxation time. This in turn proves that the reversal of the ^{7}Li NMR line broadening is the reversal of the incoherent PRE effect that is modulated by T_m, under the relevant experimental conditions described here. It is also apparent that the shortening of T_m concurs with increasing electron spin saturation, as will be further discussed. This is the basis for our debut of the acronym REPRESSION for this newly discovered effect of the reversal of the PRE by electron spin saturation, as forecasted in Introduction.

Finally, a similar trend in the paramagnetic dipolar shift is observed (see Figure S3, SI) under the influence of μw irradiation. Plots of reversal of the paramagnetic dipolar shift against different μw parameters show equivalent rates of changes as the REPRESSION effect. We note that the reversal of the PE overall is mediated by the saturation of the electron

DOI: 10.1021/acs.jpcc.8b00312
J. Phys. Chem. C 2018, 122, 5578−5589

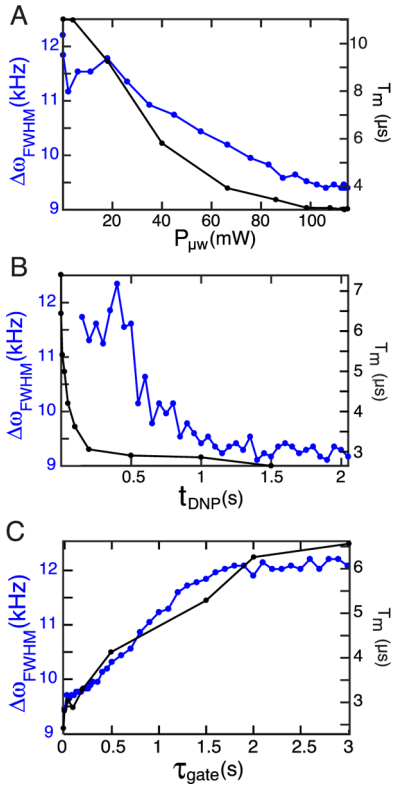

Figure 7. Electron T_m (black) and ^{7}Li NMR signal line widths (blue) as a function of μw parameters (A) μw power, (B) irradiation time, and (C) gating period using the pulse sequences shown in Figures 5A and 1A, respectively. In all of the experiments, the μw frequency is fixed at 193.75 GHz and REPRESSION time is set to 0 s. Li-electrolyte solution doped with 60 mM TEMPOmet was used as sample.

spins. In the case of REPRESSION, it is the T_m, whereas in the case of the reversal of the paramagnetic dipolar shift, it is the random reduction of the electron polarization that governs the process.

DISCUSSION

A complete understanding of the bulk nuclear polarization enhancement via DNP and its effect on the spectral features of the amplified NMR signal requires a comprehensive knowledge of the e−n, e−e, and n−n interactions at play, as well as the nuclear and electron spin relaxation rates modulated by a combination of these interactions. This is because the paramagnetic centers used as DNP polarizing agents not only induce NMR signal enhancements, but also affect the line widths and chemical shifts of the NMR spectra. As the focus of this study is the reversal of the paramagnetic effect (PE) to detect narrow lines and unambiguous peak positions in the DNP-enhanced NMR spectra in the presence of paramagnetic sites, it is important to analyze the effects of e−n couplings on $\Delta\omega_{FWHM}$ and $\Delta\delta$. The mechanism of NMR line broadening by the PE is mediated by either a coherent evolution of the spin system under e−n dipolar couplings or the relaxation enhancements of T_{2n} caused by the PRE effect. If reversal of the PE is the goal, one must achieve to suppress one or both of these mechanisms.

This study shows that under the influence of μw irradiation at liquid-helium temperature and high magnetic field, the PE, both the NMR line broadening and peak shift, can be effectively reversed. Using a series of experiments, we first confirm that the apparent reversal of the PE is not a consequence of selective DNP enhancement nor sample heating. This led us suggest that the reversal of the PE is due to apparent hyperfine decoupling (hfDC). In the literature, coherent averaging-based hfDC schemes have been reported in EPR,[62−64] which successfully averages out the e−n interaction to provide resolution enhancements in EPR hyperfine spectroscopy experiments, such as ESEEM and HYSCORE. However, these methods reported in the literature utilize high-power μw irradiation and are shown to be effective in a regime where the μw nutation frequency is much greater than the strength of the e−n interactions[62] In our case, the experimental conditions are far from conditions operational for such mechanisms. The nutation frequency achieved by 120 mW μw power falls in the range of 0.3−0.6 MHz, which is of similar strength to the e−n interactions at such high radical concentration and low temperatures. The only possibility of coherent averaging under these low μw power conditions is "self-decoupling", as assisted by much stronger e−e interactions that can truncate the relatively weak e−n interactions.[59,73,74] However, the role of μw irradiation and EPR saturation is not well understood for this mechanism. So, self-decoupling effects are likely present in our samples system in the absence of μw irradiation, but verification and understanding of their roles require further studies.

The experimental results connote that μw irradiation under the conditions of this study saturates a significant portion of the EPR spectrum, even with low μw power and short irradiation times and that the magnitude of the apparent hfDC effect concurs with the extent of electron spin saturation. The frequency profile shown in Figure 2C is the first indication of this phenomenon, in which the $\Delta\omega_{FWHM}$ is affected by the μw irradiation even at $\omega_{\mu w}$ = 193.4 GHz, i.e., 0.5 MHz apart from the EPR center. In fact, the influence of μw irradiation on the line widths and chemical shifts start at a μw irradiation frequency as far as $\omega_{\mu w}$ = 191.7 GHz (see Figure S2). The second evidence can be observed from the ε versus $P_{\mu w}$ data shown in Figure 4A (red), which indicates the presence of an oversaturation of the EPR pattern.[68,71] The oversaturation behavior arises due to the indirect cross effect DNP,[67] in which the enhancement in nuclear polarization is a result of polarization difference between two unpaired electron spins fulfilling the cross-effect condition $\Delta\omega_e = \pm\omega_n$. These electron spins fulfilling the CE are not necessarily the ones irradiated by microwaves, but indirectly depolarized due to electron spectral diffusion across an inhomogeneously broadened EPR line, as discussed by Siaw et al.[71] In the presence of strong electron spectral diffusion, the saturation of the EPR line becomes sufficiently broad to result in a reduced polarization gradient for the electron spins of the CE pair, leading to a reduced DNP enhancement.[67,71] Finally, the ELDOR data (Figure 6) indicate that the echo intensities at 193.75 GHz are affected by the μw irradiation in the range as wide as ω_{pump} = 192.8−194.6 GHz spanning 800 MHz, using a pump pulse duration of only 100 ms. This result is in agreement with the observed change in the PE with far off-resonance μw irradiations (see Figure S2 in SI). Such prominent EPR saturation can be partly ascribed to the long T_{1e} (Figure 6C), which provide sufficient time for the e−e spin interaction mediated by efficient spectral diffusion to saturate a broad portion of the EPR pattern. The efficiency of the electron spectral diffusion process can be further gleaned from the short T_{sd} time constants, as derived from the fast

DOI: 10.1021/acs.jpcc.8b00312
J. Phys. Chem. C 2018, 122, 5578−5589

components of the saturation recovery T_{1e} data (Figure S4). These results imply that the saturation of the EPR spins is assisting the hfDC effect.

The key question we sought to clarify then was whether the apparent hfDC is due to the extent of electron spin saturation reflecting the rapid spin flip-flop transitions driven by μw irradiation that averages out the coherent paramagnetic line broadening or whether the extent of electron spin saturation modulates the electron-nuclear correlation time, and so reverses the incoherent paramagnetic dipolar line broadening. Our study unequivocally shows that the latter is the case, among others based on the variation of $\Delta\omega_{FWHM}$ with the gating time, τ_{gate}, between μw irradiation and NMR detection. The narrowed ^{7}Li NMR line by hfDC broadens with increasing τ_{gate}, but not instantaneously (Figure 2C). Notably, the NMR line broadening observed in this study with increasing τ_{gate} duration differs from the reported increase in $T_{1\rho}$ and by extension of NMR line narrowing with increasing τ_{gate} time by Bornet et al. under dissolution DNP conditions.[75] The recovery of $\Delta\omega_{FWHM}$ to its original broadened value takes up to ~2 s after turning off the μw power (Figure 4C). We can reconcile this with empirical evidence that the recovery of electron spin saturation to equilibrium after turning off μw irradiation is a similarly slow process (see Figure 6B).

The e−n decoupling demonstrated by Barnes and coworkers also ascribes the seen line narrowing to EPR saturation. However, the mechanism of the line narrowing may be fundamentally different from the one observed here, as we have concluded that in our studies the electron spin saturation is truncating the incoherent PE effect, i.e., the PRE effect on the nuclear T_{2n}. To comprehend the role of electron spin saturation in the REPRESSION effect, we first need to understand the mechanism of the PRE effect. In the PRE studies used in solid-state NMR, the Solomon−Bloembergen (SB) equation[76] employed with the correlation time of the local field fluctuations at the nuclear sites caused by the paramagnetic centers is approximately considered to be equal to T_{1e}. However, the standard descriptions of the PRE effects are based on the high-temperature approximation, under which the correlation times of the local field fluctuations are short enough to satisfy the Redfield limit. At very low temperatures and when T_{1e} is very high (>100 ms), the mechanism underlying PRE is unclear. Furthermore, we observe a change in the REPRESSION effect with the EPR saturation time and the gating delay (see Figure 2B,C); these parameters cannot affect the T_{1e} because by longer duration or stronger μw irradiation, we simply take the electron spins away from the thermal equilibrium, while T_{1e} is basically the rate of returning electron spin polarization back to the thermal equilibrium. Therefore, simply changing the electron spin polarization (or saturation) cannot modulate T_{1e}. The T_m value, on the other hand, gets affected considerably by altered electron spin polarization (or saturation), as shown in Figure 7. This is the key empirical observation that supports the hypothesis that the T_m of the electron spin plays a dominating role in modulating the correlation time of the local field fluctuations under such conditions. In fact, the theoretical basis for the mechanism of T_m at relatively high electron spin concentrations at liquid-helium temperatures and high magnetic fields has been recently formulated in the literature as the spin bath quenching mechanism. In this process, the e−e flip-flop fluctuations are suppressed in the fully polarized electron spin bath that quenches the driving mechanism of the dephasing of the excited electron spins constituting an echo.[69,77] We note that in pulsed EPR of nitroxide radicals at high magnetic fields, the narrow excitation bandwidth results in the majority of the electron spin bath surrounding the excited electron spins to be unexcited. In the literature, spin bath quenching has been shown to be truncated by elevating the sample temperature, where the temperature dependence of T_m is shown to depend on the electron flip-flop rate, W. This theory has even been used to quantify local average interelectron spin distances from W derived from temperature-dependent spin bath quenching experiments.[69] In this work, we show that spin bath quenching can also be truncated by electron spin saturation that increases the electron spin temperature. This effect alone, the modulation of electron spin phase memory time, T_m, by the physical and spin temperature is a new discovery of this study, may find interesting applications in the future.

A detailed analysis of the origin of the pNMR shifts and their dependence on the μw parameters is beyond the scope of the present work. There have been a number of theoretical studies to describe the effects of Fermi contact (FC) interaction, anisotropic dipolar interaction, and spin−orbit interactions on the NMR chemical shifts by quantum mechanical calculations.[50,51] Here, we report on the experimental results demonstrating a reversal in the pNMR shifts under the influence of μw irradiation as shown in SI (Figure S3). The reversal of the pNMR shift as a function of the μw parameters also follows the same trend of the modulation in EPR saturation as the REPRESSION effect. On the basis of this observation, we postulate that a reduction in the electron spin polarization caused by the EPR saturation is responsible for the pNMR reversal. The polarization of the electron spins is very high, near unity, under the given conditions, which can be reduced significantly by μw irradiation due to the presence of a strong e−e coupling network. This leads to a reduction in the magnetic susceptibility, and hence reversal of pNMR shifts.[53]

CONCLUSIONS

Our studies demonstrate that the REPRESSION effect can significantly reverse the PRE effect using μw irradiation with only $P_{\mu w}$ = 120 mW yielding μw amplitude (ω_{1S} = 0.5 MHz), whereas the EPR spectrum of the nitroxide radicals is as broad as ~1 GHz at the base. We provide experimental evidences showing that the REPRESSION effect is driven by EPR saturation elevating the spin temperature that shortens the electron T_m. On the basis of these results, we conclude that long T_{1e} combined with a strong e−e interaction network can assist in achieving significant saturation of the EPR pattern, which can lower the T_m of the electron spins leading to the REPRESSION effect. We furthermore report that the pNMR shifts are also reversed in the same fashion as the PRE effect under the influence of the μw irradiation, which is a result of reduction in the total magnetic susceptibility modulated by the change in net electron spin polarization caused by the EPR saturation. We refer to the reversal of the PRE and pNMR shifts by electron spin saturation as REversal of Paramagnetic Effects ALtogether (REPEAL). The immediate impact of the REPEAL effect is the detection of undistorted NMR signal of nuclear spins in the proximity of paramagnetic centers. Ongoing studies of ours hint at the possibility that REPEAL by electron spin saturation is applicable beyond nitroxide radicals to transition-metal centers and can be utilized to identify the origin of the DNP-enhanced NMR signal from proximal, in contrast to remote, nuclear spins with respect to

DOI: 10.1021/acs.jpcc.8b00312
J. Phys. Chem. C 2018, 122, 5578−5589

the paramagnetic centers. The future prospects for application of the REPEAL effects are manifold: the reversal of the PE will be useful for the NMR characterization of and around paramagnetic catalytic or otherwise active paramagnetic centers, while the REPRESSION effect may enhance the resolution for NMR imaging at ultralow temperatures, as proposed by Tycko,[78] where the image resolution is limited by the static NMR line width and sensitivity. Our study shows that the design principle for minimizing the PE is maximizing electron spin saturation, which may be achieved by the design of the paramagnetic agents and sample conditions, the manipulation of μw irradiation by arbitrary pulse shaping, as well as the increased μw pulse power.

■ ASSOCIATED CONTENT

Supporting Information

The Supporting Information is available free of charge on the ACS Publications website at DOI: 10.1021/acs.jpcc.8b00312.

Radical concentration vs PE for TEMPO; $\Delta\omega_{FWHM}$ at different μw frequencies far from the EPR center; pNMR shifts as a function of μw parameters (power, time, and gating period); T_{1e} measurement for 60 mM TEMPO-met; and fitting simulations for $\Delta\omega_{FWHM}$ vs t_{DNP} and τ_{gate} and for the EPR saturation recovery experiments (PDF)

■ AUTHOR INFORMATION

Corresponding Author

*E-mail: songi@chem.ucsb.edu.

ORCID

Ilia Kaminker: 0000-0002-3527-7822

Songi Han: 0000-0001-6489-6246

Present Address

[⊥]JEOL USA Inc.,10 Dearborn Road, Peabody, Massachusetts 01960, United States (S.H.).

Author Contributions

[‖]S.K.J. and T.A.S. contributed equally.

Author Contributions

The manuscript was written through contributions of all authors. All authors have given approval to the final version of the manuscript.

Notes

The authors declare no competing financial interest.

■ ACKNOWLEDGMENTS

This study was supported by grants of the National Science Foundation (CHE #1505038 and MCB #1244651), National Institute of Health, and National Institute of Biomedical Imaging and Bioengineering (R21 #EB022731). Materials used in this study were purchased using the JEOL gift fund by the postdoctoral appointment of T.A.S. I.K. acknowledges the support of the long-term postdoctoral fellowship by the Human Frontier Science Foundation.

■ REFERENCES

(1) Lesage, A.; et al. Surface Enhanced NMR Spectroscopy by Dynamic Nuclear Polarization. *J. Am. Chem. Soc.* **2010**, *132*, 15459−15461.

(2) Griffin, R. G. Spectroscopy: Clear Signals from Surfaces. *Nature* **2010**, *468*, 381−382.

(3) Rossini, A. J.; Zagdoun, A.; Lelli, M.; Gajan, D.; Rascon, F.; Rosay, M.; Maas, W. E.; Coperet, C.; Lesage, A.; Emsley, L. One Hundred Fold Overall Sensitivity Enhancements for Silicon-29 NMR Spectroscopy of Surfaces by Dynamic Nuclear Polarization with CPMG Acquisition. *Chem. Sci.* **2012**, *3*, 108−115.

(4) Vitzthum, V.; et al. Dynamic Nuclear Polarization of Quadrupolar Nuclei Using Cross Polarization from Protons: Surface-Enhanced Aluminium-27 NMR. *Chem. Commun.* **2012**, *48*, 1988−1990.

(5) Blanc, F.; Sperrin, L.; Jefferson, D. A.; Pawsey, S.; Rosay, M.; Grey, C. P. Dynamic Nuclear Polarization Enhanced Natural Abundance ^{17}O Spectroscopy. *J. Am. Chem. Soc.* **2013**, *135*, 2975−2978.

(6) Lafon, O.; Thankamony, A. S. L.; Rosay, M.; Aussenac, F.; Lu, X.; Trebosc, J.; Bout-Roumazeilles, V.; Vezin, H.; Amoureux, J.-P. Indirect and Direct ^{29}Si Dynamic Nuclear Polarization of Dispersed Nanoparticles. *Chem. Commun.* **2013**, *49*, 2864−2866.

(7) Rossini, A. J.; Zagdoun, A.; Lelli, M.; Lesage, A.; Copéret, C.; Emsley, L. Dynamic Nuclear Polarization Surface Enhanced NMR Spectroscopy. *Acc. Chem. Res.* **2013**, *46*, 1942−1951.

(8) Guo, Z.; Kobayashi, T.; Wang, L.-L.; Goh, T. W.; Xiao, C.; Caporini, M. A.; Rosay, M.; Johnson, D. D.; Pruski, M.; Huang, W. Selective Host-Guest Interaction between Metal Ions and Metal-Organic Frameworks Using Dynamic Nuclear Polarization Enhanced Solid-State NMR Spectroscopy. *Chem. − Eur. J.* **2014**, *20*, 16308−16313.

(9) Lee, D.; Duong, N. T.; Lafon, O.; De Paëpe, G. Primostrato Solid-State NMR Enhanced by Dynamic Nuclear Polarization: Pentacoordinated Al^{3+} Ions Are Only Located at the Surface of Hydrated Γ-Alumina. *J. Phys. Chem. C* **2014**, *118*, 25065−25076.

(10) Pourpoint, F.; et al. Probing ^{27}Al-^{13}C Proximities in Metal-Organic Frameworks Using Dynamic Nuclear Polarization Enhanced NMR Spectroscopy. *Chem. Commun.* **2014**, *50*, 933−935.

(11) Lund, A.; Hsieh, M.-F.; Siaw, T.-A.; Han, S.-I. Direct Dynamic Nuclear Polarization Targeting Catalytically Active ^{27}Al Sites. *Phys. Chem. Chem. Phys.* **2015**, *17*, 25449−25454.

(12) Perras, F. A.; Kobayashi, T.; Pruski, M. Natural Abundance ^{17}O DNP Two-Dimensional and Surface-Enhanced NMR Spectroscopy. *J. Am. Chem. Soc.* **2015**, *137*, 8336−8339.

(13) Lelli, M.; et al. Fast Characterization of Functionalized Silica Materials by Silicon-29 Surface-Enhanced NMR Spectroscopy Using Dynamic Nuclear Polarization. *J. Am. Chem. Soc.* **2011**, *133*, 2104−2107.

(14) Lelli, M.; Rossini, A. J.; Casano, G.; Ouari, O.; Tordo, P.; Lesage, A.; Emsley, L. Hydrophobic Radicals Embedded in Neutral Surfactants for Dynamic Nuclear Polarization of Aqueous Environments at 9.4 Tesla. *Chem. Commun.* **2014**, *50*, 10198−10201.

(15) Song, C.; Hu, K.-N.; Joo, C.-G.; Swager, T. M.; Griffin, R. G. TOTAPOL: A Biradical Polarizing Agent for Dynamic Nuclear Polarization Experiments in Aqueous Media. *J. Am. Chem. Soc.* **2006**, *128*, 11385−11390.

(16) Matsuki, Y.; et al. Dynamic Nuclear Polarization with a Rigid Biradical. *Angew. Chem., Int. Ed.* **2009**, *48*, 4996−5000.

(17) Dane, E. L.; Maly, T.; Debelouchina, G. T.; Griffin, R. G.; Swager, T. M. Synthesis of a BDPA-TEMPO Biradical. *Org. Lett.* **2009**, *11*, 1871−1874.

(18) Griffin, R. G.; Prisner, T. F. High Field Dynamic Nuclear Polarization-the Renaissance. *Phys. Chem. Chem. Phys.* **2010**, *12*, 5737−5740.

(19) Dane, E. L.; Corzilius, B.; Rizzato, E.; Stocker, P.; Maly, T.; Smith, A. A.; Griffin, R. G.; Ouari, O.; Tordo, P.; Swager, T. M. Rigid Orthogonal Bis-TEMPO Biradicals with Improved Solubility for Dynamic Nuclear Polarization. *J. Org. Chem.* **2012**, *77*, 1789−1797.

(20) Zagdoun, A.; et al. A Slowly Relaxing Rigid Biradical for Efficient Dynamic Nuclear Polarization Surface-Enhanced NMR Spectroscopy: Expeditious Characterization of Functional Group Manipulation in Hybrid Materials. *J. Am. Chem. Soc.* **2012**, *134*, 2284−2291.

(21) Marin-Montesinos, I.; Paniagua, J. C.; Vilaseca, M.; Urtizberea, A.; Luis, F.; Feliz, M.; Lin, F.; Van Doorslaer, S.; Pons, M. Self-Assembled Trityl Radical Capsules–Implications for Dynamic Nuclear Polarization. *Phys. Chem. Chem. Phys.* **2015**, *17*, 5785−5794.

(22) Michaelis, V. K.; Smith, A. A.; Corzilius, B.; Haze, O.; Swager, T. M.; Griffin, R. G. High-Field ^{13}C Dynamic Nuclear Polarization with a Radical Mixture. *J. Am. Chem. Soc.* **2013**, *135*, 2935−2938.
(23) Sauvée, C.; Rosay, M.; Casano, G.; Aussenac, F.; Weber, R. T.; Ouari, O.; Tordo, P. Highly Efficient, Water-Soluble Polarizing Agents for Dynamic Nuclear Polarization at High Frequency. *Angew. Chem., Int. Ed.* **2013**, *52*, 10858−10861.
(24) Yau, W.-M.; Thurber, K. R.; Tycko, R. Synthesis and Evaluation of Nitroxide-Based Oligoradicals for Low-Temperature Dynamic Nuclear Polarization in Solid State NMR. *J. Magn. Reson.* **2014**, *244*, 98−106.
(25) Zagdoun, A.; et al. Non-Aqueous Solvents for DNP Surface Enhanced NMR Spectroscopy. *Chem. Commun.* **2012**, *48*, 654−656.
(26) Elisei, E.; Filibian, M.; Carretta, P.; Colombo Serra, S.; Tedoldi, F.; Willart, J. F.; Descamps, M.; Cesaro, A. Dynamic Nuclear Polarization of a Glassy Matrix Prepared by Solid State Mechanochemical Amorphization of Crystalline Substances. *Chem. Commun.* **2015**, *51*, 2080−2083.
(27) Chen, A. P.; Tan, C.; Cunningham, C. H. In *Using Pyruvic Acid as a Solvent for Dynamic Nuclear Polarization Sample Preparation*, Proceedings of the 20th Annual Meeting of ISMRM, Melborne, Australia, 2012.
(28) Becerra, L. R.; Gerfen, G. J.; Temkin, R. J.; Singel, D. J.; Griffin, R. G. Dynamic Nuclear Polarization with a Cyclotron Resonance Maser at 5 T. *Phys. Rev. Lett.* **1993**, *71*, 3561−3564.
(29) Becerra, L. R.; et al. A Spectrometer for Dynamic Nuclear Polarization and Electron Paramagnetic Resonance at High Frequencies. *J. Magn. Reson., Ser. A* **1995**, *117*, 28−40.
(30) Gerfen, G. J.; Becerra, L. R.; Hall, D. A.; Griffin, R. G.; Temkin, R. J.; Singel, D. J. High Frequency (140 GHz) Dynamic Nuclear Polarization: Polarization Transfer to a Solute in Frozen Aqueous Solution. *J. Chem. Phys.* **1995**, *102*, 9494−9497.
(31) Bajaj, V. S.; Hornstein, M. K.; Kreischer, K. E.; Sirigiri, J. R.; Woskov, P. P.; Mak-Jurkauskas, M. L.; Herzfeld, J.; Temkin, R. J.; Griffin, R. G. 250 GHz CW Gyrotron Oscillator for Dynamic Nuclear Polarization in Biological Solid State NMR. *J. Magn. Reson.* **2007**, *189*, 251−79.
(32) Pike, K. J.; et al. A Spectrometer Designed for 6.7 and 14.1 T DNP-Enhanced Solid-State MAS NMR Using Quasi-Optical Microwave Transmission. *J. Magn. Reson.* **2012**, *215*, 1−9.
(33) Smith, A. A.; Corzilius, B.; Bryant, J. A.; DeRocher, R.; Woskov, P. P.; Temkin, R. J.; Griffin, R. G. A 140 GHz Pulsed EPR/212 MHz NMR Spectrometer for DNP Studies. *J. Magn. Reson.* **2012**, *223*, 170−179.
(34) Rosay, M.; Blank, M.; Engelke, F. Instrumentation for Solid-State Dynamic Nuclear Polarization with Magic Angle Spinning NMR. *J. Magn. Reson.* **2016**, *264*, 88−98.
(35) Siaw, T. A.; Leavesley, A.; Lund, A.; Kaminker, I.; Han, S. A Versatile and Modular Quasi Optics-Based 200 GHz Dual Dynamic Nuclear Polarization and Electron Paramagnetic Resonance Instrument. *J. Magn. Reson.* **2016**, *264*, 131−153.
(36) Can, T. V.; Ni, Q. Z.; Griffin, R. G. Mechanisms of Dynamic Nuclear Polarization in Insulating Solids. *J. Magn. Reson.* **2015**, *253*, 23−35.
(37) Corzilius, B.; Smith, A. A.; Griffin, R. G. Solid Effect in Magic Angle Spinning Dynamic Nuclear Polarization. *J. Chem. Phys.* **2012**, *137*, No. 054201.
(38) Hovav, Y.; Feintuch, A.; Vega, S. Theoretical Aspects of Dynamic Nuclear Polarization in the Solid State—the Solid Effect. *J. Magn. Reson.* **2010**, *207*, 176−189.
(39) Hovav, Y.; Feintuch, A.; Vega, S. Theoretical Aspects of Dynamic Nuclear Polarization in the Solid State—the Cross Effect. *J. Magn. Reson.* **2012**, *214*, 29−41.
(40) Hovav, Y.; Feintuch, A.; Vega, S. Theoretical Aspects of Dynamic Nuclear Polarization in the Solid State-Spin Temperature and Thermal Mixing. *Phys. Chem. Chem. Phys.* **2013**, *15*, 188−203.
(41) Hovav, Y.; Levinkron, O.; Feintuch, A.; Vega, S. Theoretical Aspects of Dynamic Nuclear Polarization in the Solid State: The Influence of High Radical Concentrations on the Solid Effect and Cross Effect Mechanisms. *Appl. Magn. Reson.* **2012**, *43*, 21−41.
(42) Hu, K.-N.; Debelouchina, G. T.; Smith, A. A.; Griffin, R. G. Quantum Mechanical Theory of Dynamic Nuclear Polarization in Solid Dielectrics. *J. Chem. Phys.* **2011**, *134*, No. 125105.
(43) Hu, K.-N.; Song, C.; Yu, H.-h.; Swager, T. M.; Griffin, R. G. High-Frequency Dynamic Nuclear Polarization Using Biradicals: A Multifrequency EPR Lineshape Analysis. *J. Chem. Phys.* **2008**, *128*, No. 052302.
(44) Maly, T.; et al. Dynamic Nuclear Polarization at High Magnetic Fields. *J. Chem. Phys.* **2008**, *128*, No. 052211.
(45) Smith, A. A.; Corzilius, B.; Barnes, A. B.; Maly, T.; Griffin, R. G. Solid Effect Dynamic Nuclear Polarization and Polarization Pathways. *J. Chem. Phys.* **2012**, *136*, No. 015101.
(46) Thurber, K. R.; Tycko, R. Theory for Cross Effect Dynamic Nuclear Polarization under Magic-Angle Spinning in Solid State Nuclear Magnetic Resonance: The Importance of Level Crossings. *J. Chem. Phys.* **2012**, *137*, No. 084508.
(47) Thurber, K. R.; Tycko, R. On Mechanisms of Dynamic Nuclear Polarization in Solids. *Isr. J. Chem.* **2014**, *54*, 39−46.
(48) Thurber, K. R.; Tycko, R. Perturbation of Nuclear Spin Polarizations in Solid State NMR of Nitroxide-Doped Samples by Magic-Angle Spinning without Microwaves. *J. Chem. Phys.* **2014**, *140*, No. 184201.
(49) Wenckebach, W. T. The Solid Effect. *Appl. Magn. Reson.* **2008**, *34*, 227−235.
(50) Van den Heuvel, W.; Soncini, A. NMR Chemical Shift in an Electronic State with Arbitrary Degeneracy. *Phys. Rev. Lett.* **2012**, *109*, No. 073001.
(51) Pennanen, T. O.; Vaara, J. Nuclear Magnetic Resonance Chemical Shift in an Arbitrary Electronic Spin State. *Phys. Rev. Lett.* **2008**, *100*, No. 133002.
(52) Martin, B.; Autschbach, J. Temperature Dependence of Contact and Dipolar NMR Chemical Shifts in Paramagnetic Molecules. *J. Chem. Phys.* **2015**, *142*, No. 054108.
(53) Koehler, J.; Meiler, J. Expanding the Utility of NMR Restraints with Paramagnetic Compounds: Background and Practical Aspects. *Prog. Nucl. Magn. Reson. Spectrosc.* **2011**, *59*, 360−389.
(54) Clore, G. M.; Iwahara, J. Theory, Practice and Applications of Paramagnetic Relaxation Enhancement for the Characterization of Transient Low-Population States of Biological Macromolecules and Their Complexes. *Chem. Rev.* **2009**, *109*, 4108−4139.
(55) Corzilius, B.; Andreas, L. B.; Smith, A. A.; Ni, Q. Z.; Griffin, R. G. Paramagnet Induced Signal Quenching in MAS-DNP Experiments in Frozen Homogeneous Solutions. *J. Magn. Reson.* **2014**, *240*, 113−123.
(56) Hoff, D. E. M.; Albert, B. J.; Saliba, E. P.; Scott, F. J.; Choi, E. J.; Mardini, M.; Barnes, A. B. Frequency Swept Microwaves for Hyperfine Decoupling and Time Domain Dynamic Nuclear Polarization. *Solid State Nucl. Magn. Reson.* **2015**, *72*, 79−89.
(57) Ernst, M.; Verhoeven, A.; Meier, B. H. High-Speed Magic-Angle Spinning ^{13}C MAS NMR Spectra of Adamantane: Self-Decoupling of the Heteronuclear Scalar Interaction and Proton Spin Diffusion. *J. Magn. Reson.* **1998**, *130*, 176−185.
(58) Ernst, M.; Zimmermann, H.; Meier, B. H. A Simple Model for Heteronuclear Spin Decoupling in Solid-State NMR. *Chem. Phys. Lett.* **2000**, *317*, 581−588.
(59) Ernst, M. Heteronuclear Spin Decoupling in Solid-State NMR under Magic-Angle Sample Spinning. *J. Magn. Reson.* **2003**, *162*, 1−34.
(60) De Paëpe, G.; Eléna, B.; Emsley, L. Characterization of Heteronuclear Decoupling through Proton Spin Dynamics in Solid-State Nuclear Magnetic Resonance Spectroscopy. *J. Chem. Phys.* **2004**, *121*, 3165−3180.
(61) Leskes, M.; Thakur, R. S.; Madhu, P. K.; Kurur, N. D.; Vega, S. Bimodal Floquet Description of Heteronuclear Dipolar Decoupling in Solid-State Nuclear Magnetic Resonance. *J. Chem. Phys.* **2007**, *127*, No. 024501.
(62) Jeschke, G.; Schweiger, A. Hyperfine Decoupling in Electron Spin Resonance. *J. Chem. Phys.* **1997**, *106*, 9979−9991.

DOI: 10.1021/acs.jpcc.8b00312
J. Phys. Chem. C 2018, 122, 5578−5589

(63) Mitrikas, G.; Schweiger, A. Hyperfine Decoupling in Electron Paramagnetic Resonance as a Powerful Tool for Unraveling Complicated Eseem Spectra of S = 1/2, I ≥ 1/2 Systems. *J. Magn. Reson.* **2004**, *168*, 88−96.
(64) Van Doorslaer, S.; Schweiger, A. New Hyperfine-Decoupling Schemes in Electron Paramagnetic Resonance Spectroscopy. *Chem. Phys. Lett.* **1999**, *308*, 187−194.
(65) Kaminker, I.; Barnes, R.; Han, S. Arbitrary Waveform Modulated Pulse EPR at 200 GHz. *J. Magn. Reson.* **2017**, *279*, 81−90.
(66) Saliba, E. P.; Sesti, E. L.; Scott, F. J.; Albert, B. J.; Choi, E. J.; Alaniva, N.; Gao, C.; Barnes, A. B. Electron Decoupling with Dynamic Nuclear Polarization in Rotating Solids. *J. Am. Chem. Soc.* **2017**, *139*, 6310−6313.
(67) Hovav, Y.; Shimon, D.; Kaminker, I.; Feintuch, A.; Goldfarb, D.; Vega, S. Effects of the Electron Polarization on Dynamic Nuclear Polarization in Solids. *Phys. Chem. Chem. Phys.* **2015**, *17*, 6053−6065.
(68) Leavesley, A.; Shimon, D.; Siaw, T. A.; Feintuch, A.; Goldfarb, D.; Vega, S.; Kaminker, I.; Han, S. Effect of Electron Spectral Diffusion on Static Dynamic Nuclear Polarization at 7 Tesla. *Phys. Chem. Chem. Phys.* **2017**, *19*, 3596−3605.
(69) Edwards, D. T.; Takahashi, S.; Sherwin, M. S.; Han, S. Distance Measurements across Randomly Distributed Nitroxide Probes from the Temperature Dependence of the Electron Spin Phase Memory Time at 240 GHz. *J. Magn. Reson.* **2012**, *223*, 198−206.
(70) Berberan-Santos, M. N.; Bodunov, E. N.; Valeur, B. Mathematical Functions for the Analysis of Luminescence Decays with Underlying Distributions 1. Kohlrausch Decay Function (Stretched Exponential). *Chem. Phys.* **2005**, *315*, 171−182.
(71) Siaw, T. A.; Fehr, M.; Lund, A.; Latimer, A.; Walker, S. A.; Edwards, D. T.; Han, S.-I. Effect of Electron Spin Dynamics on Solid-State Dynamic Nuclear Polarization Performance. *Phys. Chem. Chem. Phys.* **2014**, *16*, 18694−18706.
(72) Equbal, A.; Bjerring, M.; Madhu, P. K.; Nielsen, N. C. A Unified Heteronuclear Decoupling Strategy for Magic-Angle-Spinning Solid-State NMR Spectroscopy. *J. Chem. Phys.* **2015**, *142*, No. 184201.
(73) Abragam, A.; Winter, J. *C. R. Acad. Sci.* **1959**, *249*, 1633.
(74) Bloembergen, N. On the Interaction of Nuclear Spins in a Crystalline Lattice. *Physica* **1949**, *15*, 386−426.
(75) Bornet, A.; Pinon, A.; Jhajharia, A.; Baudin, M.; Ji, X.; Emsley, L.; Bodenhausen, G.; Ardenkjaer-Larsen, J. H.; Jannin, S. Microwave-Gated Dynamic Nuclear Polarization. *Phys. Chem. Chem. Phys.* **2016**, *18*, 30530−30535.
(76) Solomon, I. Relaxation Processes in a System of Two Spins. *Phys. Rev.* **1955**, *99*, 559−565.
(77) Takahashi, S.; Hanson, R.; van Tol, J.; Sherwin, M. S.; Awschalom, D. D. Quenching Spin Decoherence in Diamond through Spin Bath Polarization. *Phys. Rev. Lett.* **2008**, *101*, No. 047601.
(78) Moore, E.; Tycko, R. Micron-Scale Magnetic Resonance Imaging of Both Liquids and Solids. *J. Magn. Reson.* **2015**, *260*, 1−9.

DOI: 10.1021/acs.jpcc.8b00312
J. Phys. Chem. C 2018, 122, 5578−5589